Critical Seed Loading from Nucleation Kinetics

Yu-Ti Tseng and Jeffrey D. Ward
Dept. of Chemical Engineering, National Taiwan University, Taipei 106-07, Taiwan

DOI 10.1002/aic.14366
Published online February 25, 2014 in Wiley Online Library (wileyonlinelibrary.com)

A method is presented for preparing critical seed loading diagrams for nonaggregating systems knowing only the nucleation kinetics. This is advantageous because it is much less time-consuming than developing and solving a complete batch process model including solubility expressions and growth rate kinetics. Furthermore, there are many more reports available in the literature of nucleation kinetics alone than there are of complete batch crystallization process models, because expressions for the nucleation rate as a function of crystal growth rate can be rapidly determined from mixed-suspension, mixed-product-removal (MSMPR) data without measuring the supersaturation. The results for 43 systems show that there is a great deal of variability in the critical seed loading, and a single correlation is inadequate to describe the relationship between critical seed loading and seed size. For a seed size of 10 μ, seed loading can effectively suppress nucleation in 92% of cases, while for seeds of size 50, 100, and 200 μ, seed loading can suppress nucleation in 74, 61, and 39% of cases, respectively. *AIChE J*, 60: 1645–1653, 2014
Keywords: batch crystallization, seed, process design

Introduction

Batch crystallization is an important and widely used operation in chemical engineering for the separation and purification of solid products. Most of the research on the operation of batch crystallization has focused on the question of how to manipulate the batch temperature (or evaporation rate or rate of antisolvent addition) with time during the batch. A recent review of developments in this field is given by Nagy and Braatz.[1]

Seeds are often introduced at the beginning of the batch, and several researchers have also investigated the effect of seed properties on batch performance.[2–7] In some cases, it has been shown that using an adequate seed loading can suppress nucleation almost entirely, which leads to a narrow, unimodal crystal size distribution (CSD). Kubota and coworkers[5–7] defined the seed loading that effectively suppresses nucleation as the critical seed loading, and proposed a correlation for critical seed loading as a function of seed size based on experimental studies of two crystallization systems.

Optimization can be used to determine a supersasturation trajectory for seeded batch crystallization. However, optimization is not well suited for determining seed loading when the objective is to minimize nucleation, because the number of nuclei and the nucleated mass will always decrease with increasing seed loading. Therefore, the optimization will suggest that an infinite seed loading is best. If a constraint is imposed on the seed loading, then the answer will always lie on the constraint.

Suppressing nucleation by increasing the seed loading is potentially an attractive option; however, all of the work conducted so far on critical seed loading has been for individual case study systems. Therefore, it remains uncertain whether increasing the seed loading can always be applied to suppress nucleation, or whether this method only works in some cases. For practical operation, there is an upper limit on the seed loading that can be used, therefore, in some cases the critical seed loading may not be practical. Models for batch crystallization kinetics and in particular expressions for nucleation rate as a function of growth rate have been published for many systems in the literature. It would be helpful if that data could be used to determine the critical seed loading for many systems, in order to determine whether seed loading can always be used to suppress nucleation or if not in what fraction of cases it can be applied. That is precisely the purpose of this work.

The remainder of this article is organized as follows: in the next section, some mathematical theory related to batch crystallization processes is reviewed, including development of models of batch crystallization, analysis of critical seed loading, and the Mullin–Nyvlt trajectory. A simple method for determining the critical seed loading as a function of seed mean size using only an expression for the nucleation rate as a function of the growth rate is also presented. In the third section, results are presented. It is shown by comparison with the solution of the complete model that the shortcut method gives a very accurate estimation of the critical seed loading. Results for the critical seed loading as a function of seed mean size for 43 systems are presented, and the effect of batch time and net crystal yield on the results is also investigated. Finally, conclusions are presented in the final section.

Theory

In this section, mathematical theory for the modeling and analysis of batch crystallization processes is presented, including

Correspondence concerning this article should be addressed to J.D. Ward at jeffward@ntu.edu.tw.

Table 1. Kinetic Parameters for the K_2SO_4–Water System from Sarkar et al.[9]

Variable	Name	Value	Units
m_{solv}	mass of solvent	3000	kg
ρ_c	density of crystal	2.66×10^{-12}	g/μm^3
k_v	volumetric shape factor	1.5	dimensionless
$k_{b,0}$	nucleation parameter	285	#/μm^3 s
B	nucleation parameter	2.25	dimensionless
$k_{g,0}$	growth parameter	1.44×10^8	μm/s
G	growth parameter	1.5	dimensionless
E_g/R	growth rate activation energy divided by gas constant	4859	K
E_b/R	nucleation rate activation energy divided by gas constant	7517	K

a batch crystallization process model, development of critical seed loading charts, derivation of the Mullin–Nyvlt trajectory, and a new shortcut method for determining the critical seed loading chart for a crystallization system knowing only the nucleation kinetics. Results are illustrated using two complete batch crystallization models: a model for the crystallization of potassium nitrate from water by Miller and Rawlings[8] (also used by Chung et al.[2]) and a model for the crystallization of potassium sulfate from water by Sarkar et al.[9]

Batch crystallization model

In the absence of agglomeration and breakage of crystals, a general expression for a population balance for a well-mixed batch crystallization system is[10]

$$\frac{\partial f(L,t)}{\partial t} + \frac{\partial (G(L,t) f(L,t))}{\partial L} = 0 \tag{1}$$

Where $f(L,t)$ is the CSD function and G is crystal growth rate (m/s). Equation 1 is subject to an initial condition based on the properties of seeds at the beginning of the batch and to a left boundary condition

$$f(0,t) = \frac{B(t)}{G(0,t)} \tag{2}$$

B is nucleation rate (#/m^{3}s). The driving force for crystal nucleation and growth is the supersaturation. In both case studies, the relative supersaturation is used

$$S = \frac{C - C_{sat}}{C_{sat}} \tag{3}$$

where C and C_{sat} are the solute concentration and saturation solute concentration in units of kg/kg solvent.

The following empirical expressions can be used for the nucleation and growth rates

$$G = k_g S^g \tag{4}$$

$$B = k_b S^b \mu_3 \tag{5}$$

where μ_3 is the third moment of CSD. and E_g and E_b are the activation energies of growth and nucleation, respectively. For the potassium sulfate process described by Sarkar et al.[9] the parameters k_b and k_g are temperature dependent

$$k_g = k_{g,0} e^{-E_g/RT} \tag{6}$$

$$k_b = k_{b,0} e^{-E_b/RT} \tag{7}$$

The values of the parameters for the potassium sulfate process model are given in Table 1. For the potassium nitrate process described by Chung et al.,[2] the parameters k_b and k_g are constant, and all model parameters for the process are given in Table 2.

The definition of the moments is

$$\mu_i = \int_0^\infty L^i f(L) dL \quad i = 0, 1, 2... \tag{8}$$

and expressions for the time evolution of the moments (if crystal growth is independent of crystal size) are

$$\frac{d\mu_0}{dt} = B \tag{9}$$

$$\frac{d\mu_i}{dt} = iG\mu_{i-1} \quad i = 1, 2, ... \tag{10}$$

An expression for a mass balance on the solute is

$$\frac{dC}{dt} = -3G\rho_c k_v \mu_2 \tag{11}$$

For the seed-grown crystals (subscript s) and nuclei-grown crystals (subscript n), the expressions are

$$\frac{d\mu_{s,0}}{dt} = 0 \tag{12}$$

$$\frac{d\mu_{s,i}}{dt} = iG\mu_{s,i-1} \quad i = 1, 2, ... \tag{13}$$

$$\frac{d\mu_{n,0}}{dt} = B \tag{14}$$

$$\frac{d\mu_{n,i}}{dt} = iG\mu_{n,i-1} \quad i = 1, 2, ... \tag{15}$$

Note that for each moment, the total crystal value equals the seed-grown value plus nuclei-grown value

$$\mu_{T,i} = \mu_{n,i} + \mu_{s,i} \tag{16}$$

Critical seed loading charts

When seeds are introduced at the start of a batch, the mass of seeds used can have a significant effect on the operation of the process. In most cases, for a given seed size and other seed properties, the nucleated mass decreases as the initial seed mass increases, and in some cases the nucleated mass can be made negligibly small if the initial seed mass is large enough.

Kubota and coworkers explored this phenomenon experimentally. They defined two parameters. The first is the

Table 2. Kinetic Parameters for the KNO_3–Water System from Chung et al.[2]

Variable	Name	Value	Units
m_{solv}	mass of solvent	7.57×10^3	kg
ρ_c	density of crystal	2.11×10^3	kg/m^3
k_v	volumetric shape factor	1	dimensionless
k_b	nucleation parameter	4.6401×10^{11}	#/m^3 s
B	nucleation parameter	1.78	dimensionless
k_g	growth parameter	1.1612×10^{-4}	m/s
G	growth parameter	1.32	dimensionless

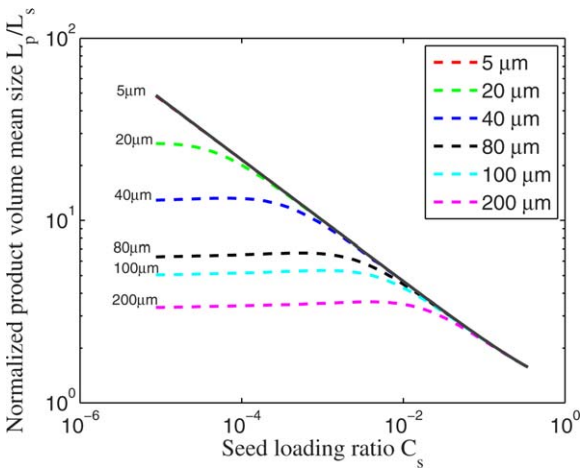

Figure 1. Seed loading chart for the potassium nitrate system.

[Color figure can be viewed in the online issue, which is available at wileyonlinelibrary.com.]

normalized product volume mean size (L_p/L_s) where L is the volume mean size (μ_4/μ_3) and the subscripts p and s refer to the final product and initial seed size, respectively. The second is the seed loading ratio ($C_s=W_s/W_{th}$) where W_s is the initial seed mass and W_{th} is the theoretical net crystal yield. W_{th} can be calculated if the initial and final solution concentrations and solvent mass w are known

$$W_{th}=w(C_0-C_f) \tag{17}$$

Kubota and coworkers performed a series of experiments in which the batch time and temperature trajectory were fixed. For a given seed size, they increased the seed mass and plotted the normalized product volume mean size vs. seed loading ratio. They then repeated the procedure for several different seed mean sizes. In the first part of this work, we follow the same procedure except that we use numerical simulation based on models of crystallization published in the literature. The result for the potassium nitrate process is shown in Figure 1, and the result for the potassium sulfate process is shown in Figure 2.

The models were solved using a linear cooling profile with zero initial supersaturation and a parabolic seed distribution with a width at the base equal to 20% of the seed mean size. For the potassium nitrate process, the temperature was reduced from 32 to 22°C, over 160 min, while for the potassium sulfate process the temperature was reduced from 50 to 30°C over 30 min.

The trend of normalized product mean size with seed loading ratio can be explained as the result of a tradeoff between two competing phenomena. At very low seed loading ratio, the seeds have little effect on the batch outcome because there are so few of them. Almost all of the product mass is from nucleated crystals, and so the product mean size is independent of seed loading at very low seed loading (the lines are flat). As seed loading increases, seeds begin to have a greater effect on the batch outcome. At very high seed loading ratio, there are so many seeds that each seed can only grow a tiny amount. Thus, the normalized product volume mean size approaches 1 in the limit of high seed loading for all seed sizes.

At intermediate seed loading, a tradeoff is observed. On the one hand, as the seed loading is increased there is less material available in solution for the growth of each seed, which tends to make the product volume mean size smaller. Conversely, nucleation is suppressed, which tends to make the product volume mean size larger. Thus, in some cases, especially for larger seed sizes, the product mean size may first increase and then decrease with increasing seed loading.

For every crystal size, if agglomeration is negligible the plot of normalized product mean size vs. seed loading approaches a common curve which Kubota and coworkers call the ideal growth curve (the solid lines in Figures 1 and 2). In this limiting case, the mass of nucleated crystals is negligible and essentially all of the material which precipitates from solution is consumed in the growth of seeds.

The shape of the ideal growth line can be derived analytically. Application of a material balance in the case where all of the solid precipitate is consumed in the growth of seeds gives

$$\frac{W_s}{k_v\rho_c L_s^3}=\frac{W_s+W_{th}}{k_v\rho_c L_p^3} \tag{18}$$

where L_s and L_p are the seed and product mean sizes, respectively, and ρ_c and k_v are the crystal density and volumetric shape factor, respectively. Equation 18 can be rearranged to give

$$\frac{L_p}{L_s}=\left(\frac{1+C_s}{C_s}\right)^{1/3} \tag{19}$$

In the limit of low seed loading

$$\frac{L_p}{L_s}=C_s^{-1/3} \tag{20}$$

Therefore, the slope of the ideal growth line approaches $-1/3$ on a logarithmic plot. Kubota and coworkers call the point (the value of the seed loading) at which the normalized product mean size curve for a given seed size becomes indistinguishable from the ideal growth line the critical seed loading, C_s^*. That is, the critical seed loading is the lowest seed loading ratio for which essentially all of the material that crystallizes out of the solution is consumed in the growth of the seeds.

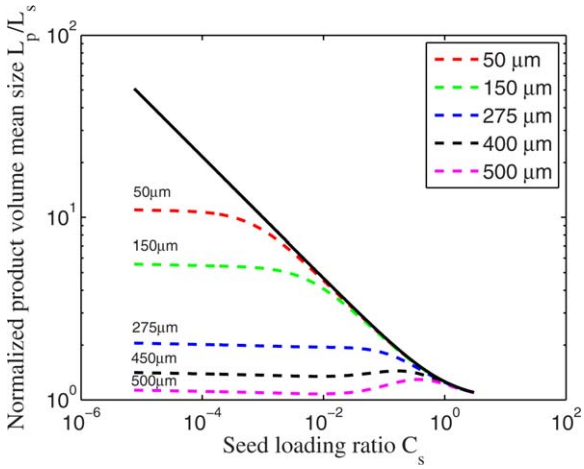

Figure 2. Seed chart for the potassium sulfate system.

[Color figure can be viewed in the online issue, which is available at wileyonlinelibrary.com.]

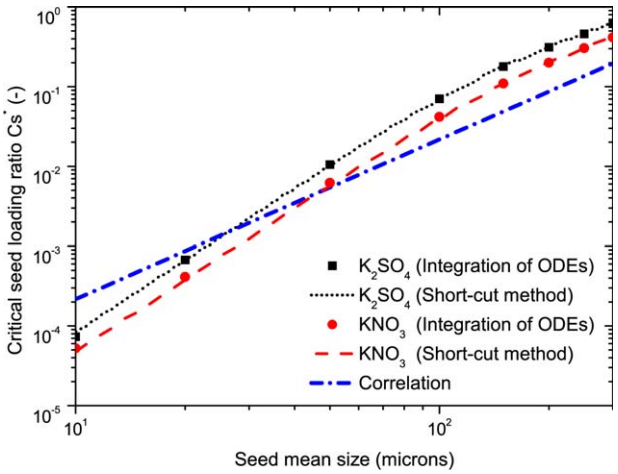

Figure 3. Critical seed loading chart for the potassium nitrate and potassium sulfate systems.

Continuous lines are determined by the shortcut method and discrete markers are determined by solving the full ODE model. The correlation for the critical seed loading due to Kubota and coworkers is also shown. [Color figure can be viewed in the online issue, which is available at wileyonlinelibrary.com.]

After the critical seed loading ratio is determined for several different seed sizes, it can be plotted vs. seed size. This chart can then serve as a guideline for process design: for a given seed size, the seed loading required to effectively suppress nucleation can be determined. Kubota and coworkers suggested the following empirical relationship between critical seed loading and seed mean size based on their experimental work

$$C_s^* = 2.17\times10^{-6} L_S^2 \tag{21}$$

where L_s is in microns.

A mathematical model such as that for the potassium nitrate and potassium sulfate systems will always predict some nonzero nucleated mass; therefore, it is necessary to make a somewhat arbitrary specification as to what constitutes "essentially" ideal growth. In this work, the criterion used was that the critical seed loading ratio was the seed loading ratio required to keep the nucleated mass below 1% of the total net crystal yield.

Mullin–Nyvlt trajectory

Mullin and Nyvlt[11] published a concentration trajectory for seeded batch crystallization. Here we briefly repeat their derivation. They made the following assumptions: (1) nucleated mass is small compared to seed-grown mass (2) growth rate is constant (independent of time and crystal size) and (3) seeds are monodisperse. With these assumptions, the seed size x as a function of time is

$$x(t) = x_0 + \tilde{G}t \tag{22}$$

where x_0 is the initial seed size, $\tilde{G}$ is the constant growth rate and t is the time during the batch. The third moment of the CSD as a function of time is

$$\mu_3(t) = n_0\left(x_0+\tilde{G}t\right)^3 \tag{23}$$

where n_0 is the number of seed crystals per unit volume of suspension. At the beginning of the batch

$$m_s = \rho_c k_v \mu_3(0) = \rho_c k_v n_0 x_0^3 \tag{24}$$

So

$$n_0 = \frac{m_s}{\rho_c k_v x_0^3} \tag{25}$$

$$\mu_3(t) = \frac{m_s}{\rho_c k_v x_0^3}\left(x_0+\tilde{G}t\right)^3 \tag{26}$$

At the end of the batch

$$C_0 - C_f = m_s\left(\left(1+\frac{\tilde{G}t_f}{x_0}\right)^3 - 1\right) \tag{27}$$

Equation 27 can be rearranged to solve for the required constant growth rate

$$\tilde{G} = \left[\left(\frac{C_0-C_f}{m_s}+1\right)^{1/3} - 1\right]\frac{x_0}{t_f} \tag{28}$$

The Mullin–Nyvlt trajectory then is

$$C(t) = C_0 - \rho_c k_v \mu_3(t) + m_s = C_0 - m_s\left(\left(1+\frac{\tilde{G}t}{x_0}\right)^3 - 1\right) \tag{29}$$

Expression for the critical seed loading ratio

Equations 9 and 15 can be integrated to determine the third moment of the nucleated crystals at the end of the batch

$$\mu_{3,n} = \int_0^{t_f} 3G\int_0^{t_4} 2G\int_0^{t_3} G\int_0^{t_2} B(t_1)\,dt_1\,dt_2\,dt_3\,dt_4 \tag{30}$$

Under the assumptions of the Mullin–Nyvlt approximation (constant growth rate, small nucleated mass), if the nucleation rate B is given by the general expression

$$B = k_b G^\gamma \mu_3^j \tag{31}$$

Then

$$\mu_{3,n} = 6k_b (n_0)^j \tilde{G}^{3+\gamma}\int_0^{t_f}\int_0^{t_4}\int_0^{t_3}\int_0^{t_2}\left(x_0+\tilde{G}t_1\right)^{3j} dt_1\,dt_2\,dt_3\,dt_4 \tag{32}$$

where n_0 is the number of seeds (Eq. 25) and $\tilde{G}$ is the constant growth rate (Eq. 28). Integration of Eq. 32 gives

$$\mu_{3,n}(t_f) = 6k_b (n_0)^j \tilde{G}^{3+\gamma}\left(\frac{\left(x_0+\tilde{G}t\right)^{3j+4}}{\tilde{G}^4\prod_{k=1}^{4}(3j+k)} - \sum_{p=0}^{3}\frac{t^m (x_0)^{3j+4-m}}{p!\tilde{G}^{4-p}\prod_{k=1}^{4-p}(3j+k)}\right) \tag{33}$$

If the maximum allowable nucleated mass, the net crystal yield (C_0-C_f) and the batch time t_f are specified, Eq. 33 provides an implicit relationship between the seed mass m_s (which appears in the expressions for n_0 and $\tilde{G}$) and seed size x_0 (which appears directly in Eq. 33 as well as in the expressions for n_0 and $\tilde{G}$). Thus the seed loading required to suppress nucleation can be determined for a given seed size.

Empirical models for the crystal growth rate such as that of Eq. 31 will always predict some nonzero nucleated mass. Therefore, in solving for the critical seed loading ratio it is

Table 3. Data for Crystallization Systems Considered in this Work.

Species	k_b[a]	γ	j	α[b]	B	R^2
Ammonium sulfate[c]	3.70×10^{15}	1.5	1	1.685×10^{-9}	2.883	1
Ammonium sulfate[c]	6.43×10^{14}	1.22	0.98	4.084×10^{-9}	2.644	0.9996
Ammonium sulfate[c]	2.90×10^{10}	1.03	0	5.289×10^{-5}	1.61	0.9972
Ammonium sulfate[c]	2.32×10^{13}	1.5	0	1.158×10^{-5}	1.788	0.998
Potassium chloride[c]	2.86×10^{21}	2.55	0	1.517×10^{-5}	1.761	0.9979
Potassium chloride[c]	2.06×10^{40}	4.99	0.14	7.574×10^{-6}	1.861	0.9982
Potassium dichromate[c]	4.58×10^{8}	0.53	0	3.770×10^{-3}	1.13	0.996
Potassium dichromate[c]	8.35×10^{6}	0.5	0.6	8.926×10^{-9}	2.691	0.9991
Potassium dichromate[c]	4.58×10^{9}	0.48	1	3.611×10^{-8}	2.724	0.9994
Potassium nitrate[c]	3.50×10^{16}	1.38	1	1.958×10^{-7}	2.462	0.9991
Potassium nitrate[c]	1.34×10^{14}	1.3	0	8.549×10^{-4}	1.297	0.9961
Potassium nitrate[c]	1.77×10^{18}	2.06	0.5	7.985×10^{-8}	2.442	0.9994
Potassium nitrate[c]	2.49×10^{17}	1.76	1	1.989×10^{-9}	2.858	1
Potassium sulfate[c]	4.44×10^{6}	0	1	7.27×10^{-12}	3.04	0.9997
Sodium chloride[c]	1.54×10^{19}	2	1	2.755×10^{-9}	2.827	0.9999
Barium nitrate[c]	1.94×10^{20}	1.82	1	9.773×10^{-7}	2.251	0.9985
Calcium carbonate[c]	3.42×10^{21}	2	0	5.75×10^{-3}	1.109	0.9968
Calcium oxalate[c]	2.28×10^{14}	1.14	0	6.166×10^{-3}	1.09	0.9966
Calcium sulfate 1/2 H_2O[c]	5.32×10^{24}	2.8	0	1.33×10^{-4}	1.515	0.997
Calcium sulfate 1/2 H_2O[c]	8.59×10^{33}	3.2	0	2.255×10^{-2}	1.007	0.9984
Silver bromide[c]	6.37×10^{49}	4	0	6.63×10^{-2}	0.886	1
Ammonium alum/H_2O/EtOH[c]	4.32×10^{18}	2	0	1.79×10^{-4}	1.477	0.9968
Ammonium alum/H_2O/EtOH[c]	2.20×10^{13}	1	0	8.085×10^{-3}	1.062	0.9967
Ammonium sulfate/H_2O/MeOH[c]	5.74×10^{37}	4	0	2.789×10^{-3}	1.195	0.9969
Sodium chloride/H_2O/EtOH[c]	2.02×10^{75}	9	0	3.308×10^{-4}	1.431	0.9971
Sodium chloride/H_2O/EtOH[c]	4.54×10^{14}	1.72	0	6.091×10^{-6}	1.862	0.9983
Sodium chloride/H_2O/EtOH[c]	1.93×10^{24}	2.4	0	2.909×10^{-3}	1.179	0.9966
Sodium chloride/H_2O/EtOH[c]	1.29×10^{65}	7.9	0	1.343×10^{-4}	1.528	0.9973
Cyclonite/HNO_3/H_2O[c]	7.02×10^{24}	2.72	0	2.855×10^{-4}	1.429	0.9967
Potassium nitrate[2]	9.40×10^{16}	1.35	1	9.376×10^{-10}	3.319	0.9997
Xylitol[13]	4.47×10^{44}	3.65	4.7	1.937×10^{-10}	2.959	0.9995
Succinic acid[14]	2.91×10^{33}	3.82	1	1.908×10^{-8}	2.611	0.9998
Potassium sulfate (high T)[d9]	3.77×10^{14}	0.967	1	1.527×10^{-5}	1.89	0.9967
Potassium sulfate (average T)	2.86×10^{14}	0.967	1	4.886×10^{-6}	2.081	0.9974
Potassium sulfate (low T)	2.12×10^{14}	0.967	1	6.426×10^{-6}	2.001	0.9967
Potassium dihydrogen phosphate[15]	2.97×10^{8}	0.565	0.943	9.329×10^{-10}	3.005	1
Potassium alum (high T)[d16]	1.12×10^{13}	1.52	1	1.149×10^{-8}	2.802	1
Potassium alum (average T)	1.28×10^{12}	1.52	1	4.883×10^{-12}	2.966	0.9998
Potassium alum (low T)	1.02×10^{11}	1.52	1	7.486×10^{-13}	3.002	0.9998
Pentaerythritol (high T)[d17]	1.04×10^{16}	2	0	9.256×10^{-7}	2.073	0.9989
Pentaerythritol (average T)	1.04×10^{16}	2	0	9.300×10^{-7}	2.072	0.9989
Pentaerythritol (low T)	1.05×10^{16}	2	0	9.352×10^{-7}	2.072	0.9989
Ammonium sulfate[18]	1.80×10^{28}	2.5	1.8	5.801×10^{-9}	3.034	0.9996

k_b, γ, and j are parameters in the nucleation rate expression $B = k_b G^{\gamma} \mu_3^j$ α and β are parameters in the best fit for a correlation of the form $C_s^* = \alpha x_0^{\beta}$, and R^2 is the goodness of fit of the correlation (See the Appendix for additional details).

[a] k_b has units of $(\#/\mathrm{L \cdot s})(\mathrm{m/s})^{-\gamma}(\mathrm{m^3/kg\ solvent})^{-j}$.

[b] α has units of $\mu\mathrm{m}^{-\beta}$.

[c] Originally reported by Garside and Shah[12].

[d] For kinetic expressions where the nucleation rate also depends temperature, effective nucleation rate constants k_b are determined using the maximum, average, and minimum value of the temperatures considered by the authors of the original work.

necessary to specify a nonzero nucleated mass fraction that constitutes "essentially" ideal growth. In this work, a nucleated mass fraction of 1% is considered to represent the case of ideal growth.

Results

To test the shortcut method (Eq. 33), the critical seed loading was determined as a function of seed size for the two case study systems (potassium nitrate and potassium sulfate) two ways: (1) using the shortcut method and (2) solving the complete batch crystallization model (Eqs. 9–15). When the complete batch crystallization model is solved, it is not necessary to assume that the crystal growth rate is constant over the batch or that the nucleated mass is small. The results are shown in Figure 3. The critical seed loading determined using the shortcut method is shown as continuous lines, and the critical seed loading determined by solving the complete batch crystallization model is shown with solid markers. The shortcut method gives results very close to those determined by solving the full crystallization model. For the potassium nitrate process, the average of the absolute value of the errors is 5.2%, while for the potassium sulfate process it is 1.4%. This suggests that the assumptions that underlie the shortcut method are reasonable and that the method gives reliable results.

The correlation recommended by Kubota and coworkers (Eq. 21) is also shown in Figure 3. The correlation is roughly consistent with the results for these two systems, although it overestimates the critical seed loading at low seed sizes and underestimates the critical seed loading at large seed sizes. There is no reason to expect that the results of the simulations should match the correlation of Kubota more closely, since the correlation was determined for one particular solute–solvent system with one crystallizer geometry and one agitation rate.

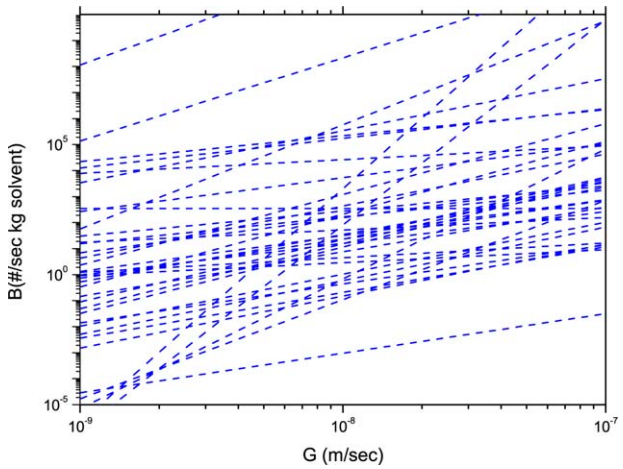

Figure 4. Nucleation rate vs. growth rate for all systems considered in this work.

The references from which the nucleation rate expressions are taken are given in Table 3. [Color figure can be viewed in the online issue, which is available at wileyonlinelibrary.com.]

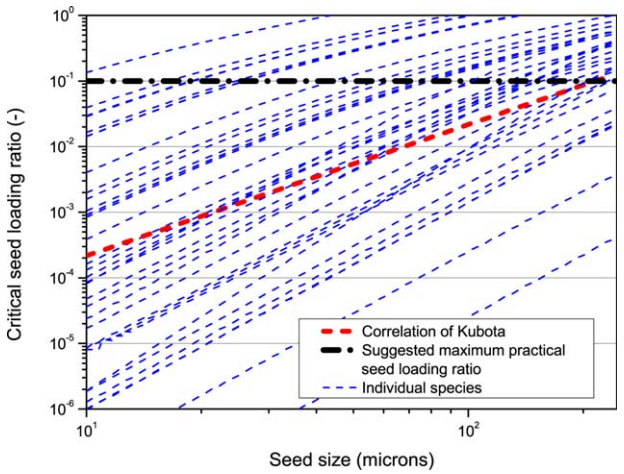

Figure 5. Critical seed loading chart for all systems considered in this work.

The practical upper limit on the seed loading ratio used in this work and the correlation of Kubota and coworkers are also shown. [Color figure can be viewed in the online issue, which is available at wileyonlinelibrary.com.]

Having demonstrated that the shortcut method gives results very similar to those developed from a complete crystallization model, we next applied the shortcut method to systems for which the nucleation rate has been determined as a function of crystal growth rate, but for which a complete batch crystallization model is not necessarily available. Table 3 shows the nucleation kinetics of all systems considered in this study. Many were originally tabulated by Garside and Shah.[12]

Figure 4 shows the nucleation rate plotted as a function of growth rate for all systems considered in this work. The figure is prepared by plotting Eq. 31 using the parameter

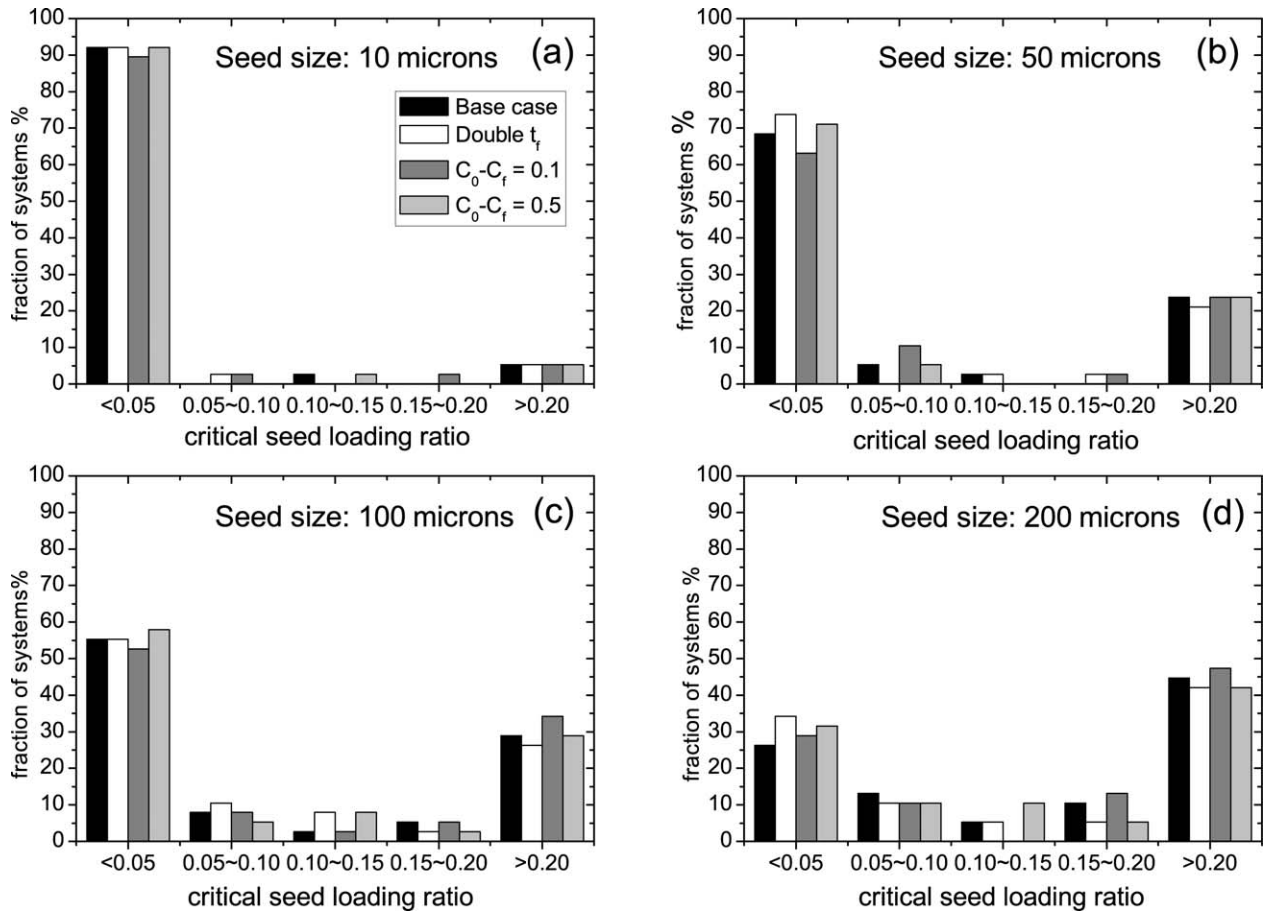

Figure 6. Effect of process variables (batch time and net crystal yield) on the distribution of critical seed loading ratio for seeds of different sizes (a) 10 μ, (b) 50 μ, (c) 100 μ, and (d) 200 μ.

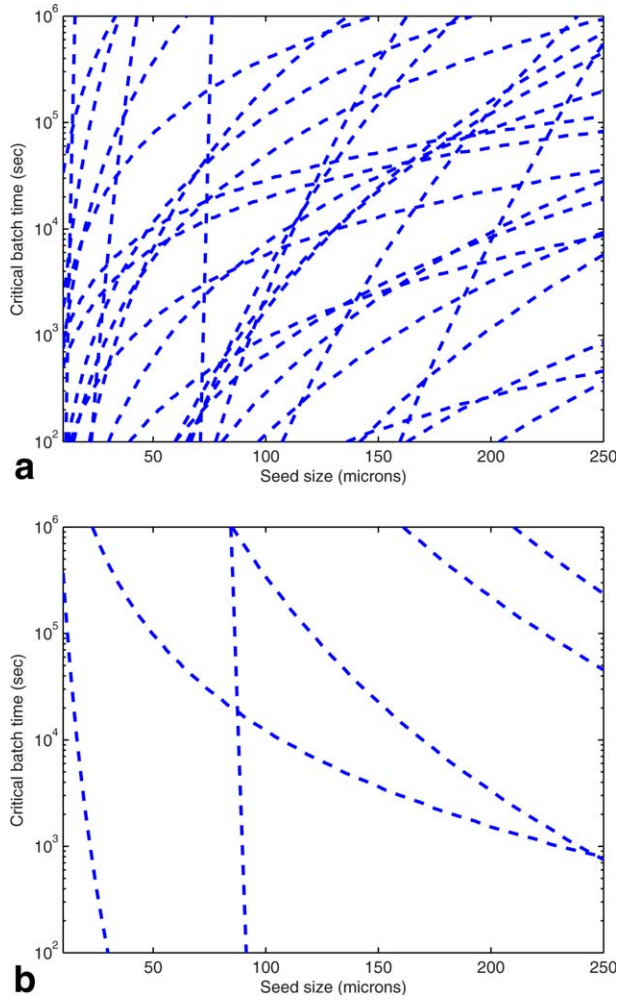

Figure 7. Critical batch time vs. seed size for all systems listed in Table 3.

The nominal batch time (2 h) is also shown. (a) Systems with $\gamma > 1$. (b) Systems with $\gamma < 1$. [Color figure can be viewed in the online issue, which is available at wileyonlinelibrary.com.]

values given in Table 3 and calculating μ_3 by assuming a solid crystal mass of 0.2 kg/kg solvent. The individual lines are not labeled for clarity; however it is clear that there is a wide variability in the nucleation rate as a function of growth rate for different systems.

Given the wide variability between different systems of the nucleation rates as a function of the growth rates, it would not be surprising if there was also great variability in the critical seed loading as a function of seed mean size. This is indeed borne out by Figure 5 which shows the critical seed loading as a function of seed mean size for all of the systems. In all cases, the critical seed loading ratio increases with seed size as expected. However, the required seed loading varies over many orders of magnitude for different systems. In real crystallization processes, there is an upper limit on the seed loading ratio for practical operation. In this work, that limit is considered to be 0.1, and the limit is also marked in Figure 5. The correlation of Kubota and coworkers is also shown in the figure. It lies roughly in the middle of the data and therefore may serve as a starting point for determining the critical seed loading ratio, although there is no guarantee that it will give an accurate result for any particular system.

Table 3 also shows parameters α and β for a critical seed loading correlation of the form $C_s^* = \alpha x_0^\beta$ when x_0 has units of microns for each of the crystal systems. The value of the exponent β ranges from 0.87 to 3.06. However, the goodness of fit (R^2) for all of the cases is very good, suggesting that a correlation of this type is suitable to describe most crystallization systems, although the coefficients are different for each system. The values of the parameters and the goodness of fit were calculated using the Curve Fitting Toolbox in Matlab. Additional details are given in the Appendix.

The data shown in Figure 5 were calculated for the case of a net crystal yield of 0.20 kg/kg solvent and a batch time of 2 h. In order to investigate the effect of these parameters on the outcome, the analysis was repeated for different values of the net crystal yield (0.10, 0.50) and batch time (4 h). The results are represented as a bar chart in Figure 6. The chart indicates the fraction of systems with a critical seed loading ratio in different ranges: <0.05, 0.05–0.10, 0.10–0.15, 0.15–0.20, and >0.20. For practical operation, a seed loading less than 0.10 is desirable. As expected, the figure shows that as the seed size increases, a higher seed loading is required to suppress nucleation. However, the figure also shows that large changes in the batch time or net crystal yield have only a small effect on the critical seed loading. As expected, increasing the batch time reduces the required seed loading ratio, but only very slightly. Changing the net crystal yield $C_0 - C_f$ may slightly increase or decrease the critical seed loading ratio depending on the system. (Note that increasing the net crystal yield always increases the critical seed mass, however, the critical seed loading ratio, defined as the critical seed mass divided by the net crystal yield, may increase or decrease.) The most important single variable affecting the critical seed loading ratio is the seed size, and for a given seed size there is great variability in the critical seed loading between different systems.

The method for estimating the critical seed loading described in this article neglects several factors that could potentially affect the outcome, including the seed injection temperature, the width of the seed CSD, the rate of cooling and supersaturation profile during the batch, and agglomeration of crystals during the batch. Although, results are not shown due to space constraints, we have investigated the effect of seed injection temperature (which is related to the initial supersaturation), the width of the seed CSD and the cooling profile. The investigations showed that these parameters effect the nucleated mass only when the seed loading is sufficiently less than the critical seed loading so that a significant mass of nucleated material forms during the batch. As the seed loading approaches the critical seed loading, a nearly identical results are observed for all reasonable supersaturation trajectories, initial supersaturation, and width of seed distribution.

The only phenomenon that may significantly affect the result that is not accounted for in the shortcut model is agglomeration. If a significant amount of agglomeration occurs, seeds may stick together in which case the effective seed size would be significantly larger than in the case of no agglomeration. This in turn would reduce the effectiveness of the seeds for inhibiting nucleation.

In this work, the batch time and net crystal yield are made the same for all systems for comparison. This means in

some cases that these parameters are significantly different from the parameters used by the original authors to produce the kinetic models. Equation 33 could also be used to solve for the "critical batch time" required for a given net crystal yield and seed loading, or the "critical net crystal yield" for a given seed loading and batch time.

To illustrate this possibility, the critical batch time was determined for all of the systems listed in Table 3 for a seed loading ratio of 5% and the same net crystal yield used to produce Figure 5 (0.2 kg/kg). The results are shown in Figure 7. Unlike critical seed loading ratio, the critical batch time estimated by Eq. 33 may either increase or decrease with seed mean size depending on the value of the exponent γ in Eq. 31. If γ is greater than one, then the nucleation rate increases more rapidly with increasing supersaturation than the growth rate. In this case, a larger batch time is preferable for suppressing nucleation and therefore the critical batch time increases with increasing seed size for a given seed loading. This is the most common case. In a few of the cases listed in Table 3, γ is less than one. In this case, a shorter batch time is preferred to suppress nucleation, and therefore, the critical batch time decreases with seed size. To emphasize this result, the data are plotted in two separate panels. Panel (a) shows the critical batch time vs. seed size for systems with $\gamma > 1$, and panel (b) shows the same plot for systems where $\gamma < 1$. If γ is nearly equal to one, then the plot of critical batch time vs. seed size is nearly vertical, indicating that adjusting the batch time is not an effective way to suppress nucleation in that case.

Conclusions

In this work, a method is presented for determining the critical seed loading ratio for a batch crystallization process knowing only the nucleation kinetics. The method permits the rapid determination of the critical seed loading ratio for many systems. The results show that there is a great variability in critical seed loading ratio for different systems. A correlation proposed by Kubota and coworkers lies near to the middle of the data but may not be accurate enough to predict the critical seed loading ratio for many systems. The critical seed loading ratio increases with seed size for all systems. Seed size is the single most important variable affecting seed loading: significant changes in the net crystal yield or batch time have only a small effect on the critical seed loading ratio.

As stated previously, an important assumption underlying this work is that agglomeration is negligible. If a significant amount of agglomeration occurs the effective seed size would be significantly larger than in the case of no agglomeration and this in turn would reduce the effectiveness of the seeds for inhibiting nucleation.

Acknowledgment

The authors wish to express their gratitude to the National Science Council of Taiwan for financial support.

Notation

B = nucleation rate, #/m^{3}s
C = concentration, kg/m^3
C_s = seed loading ratio, −
C_s^* = critical seed loading ratio, −
C_{sat} = saturated concentration, kg/m^3
E_b = nucleation activation energy, J/mol K
E_g = growth activation energy, J/mol K
f = CSD function, #/m^3 m
G = crystal growth rate, m/s
k_b = nucleation parameter, #/m^3 s
k_g = growth parameter, m/s
k_v = volumetric shape factor, −
L_p = product volume mean size, m
L_s = seed volume mean size, m
m_s = seed mass, kg
n_0 = number of seed crystals, #/m^3
S = relative supersaturation, −
t_f = final time, s
w = solvent mass, kg
W_s = seed mass, kg
W_{th} = theoretical crystal yield, kg
x_0 = seed mean size, m
μ_i = ith moment of the CSD, m^i/m^3
ρ_c = crystal density, kg/m^3

Literature Cited

1. Nagy Z K, Braatz RD. Advances and new directions in crystallization control. *Annu Rev Chem Biomol Eng*. 2012;3:55–75.
2. Chung SH, Ma DL, Braatz RD. Optimal seeding in batch crystallization. *Can J Chem Eng*. 1999;77:590–596.
3. Hojjati H, Rohani S. Cooling and seeding effect on supersaturation and final crystal size distribution (CSD) of ammonium sulphate in a batch crystallizer. *Chem Eng Process*. 2005;44:949–957.
4. Ward JD, Yu CC, Doherty MF. A new framework and a simpler method for the development of batch crystallization recipes. *AIChE J*. 2011;57:606–617.
5. Doki N, Kubota N, Yokota M, Chianese A. Determination of critical seed loading ratio for the production of crystals of uni-modal size distribution in batch cooling crystallization of potassium alum. *J Chem Eng Jpn*. 2002;35:670–676.
6. Doki N, Kubota N, Sato A, Yokota M, Hamada O, Masumi F. Scaleup experiments on seeded batch cooling crystallization of potassium alum. *AIChE J*. 1999;45:2527–2533.
7. Jagadesh D, Kubota N, Yokota M, Sato A, Tavare NS. Large and mono-sized product crystals from natural cooling mode batch crystallizer. *J Chem Eng Jpn*. 1996;29:865–873.
8. Miller SM, Rawlings JB. Model Identification And Control Strategies For Batch Cooling Crystallizers. *AIChE J*. 1994;40:1312–1327.
9. Sarkar D, Rohani S, Jutan A. Multi-objective optimization of seeded batch crystallization processes. *Chem Eng Sci*. 2006;61:5282–5295.
10. Randolph AD, Larson MA. Theory of particulate processes: analysis and techniques of continuous crystallization, 2nd ed. San Diego: Academic Press, 1988.
11. Mullin JW, Nyvlt J. Programmed cooling of batch crystallizers. *Chem Eng Sci*. 1971;26:369–377.
12. Garside J, Shah MB. Crystallization kinetics from MSMPR crystallizers. *Ind Eng Chem Proc Dev*. 1980;19:509–514.
13. Hao HX, Hou BH, Wang JK, Lin GY. Effect of solvent on crystallization behavior of xylitol. *J Cryst Growth*. 2006;290:192–196.
14. Qiu YF, Rasmuson AC. Nucleation and growth of succinic acid in a batch cooling crystallizer. *AIChE J*. 1991;37:1293–1304.
15. Yang GY, Louhi-Kultanen M, Sha ZL, Kallas J. Determination of operating conditions for controlled batch cooling crystallization. *Chem Eng Technol*. 2006;29:200–205.
16. Corriou JR, Rohani S. Nonlinear control of a batch crystallizer. *Chem Eng Commun*. 2002;189:1415–1436.
17. Bernardo A, Giulietti M. Modeling of crystal growth and nucleation rates for pentaerythritol batch crystallization. *Chem Eng Res Des*. 2010;88:1356–1364.
18. Jager J, de Wolf S, Kramer HJM, de Jong EJ. Estimation of nucleation kinetics from crystal size distribution transients of a continuous crystallizer. *Chem Eng Sci*. 1991;46:807–818.
19. The MathWorks, Inc. Curve Fitting Toolbox User's Guide. 2013.

Appendix

The values of the parameters α and β and the R-square statistic were determined using the curve-fitting toolbox in Matlab. The R-square statistic is defined as

$$R^2 = \frac{\mathrm{SSR}}{\mathrm{SST}} \tag{A1}$$

where SSR is the sum of the squares of the regression

$$\mathrm{SSR} = \sum_{i=1}^{n} w_i (\hat{y}_i - \bar{y})^2 \tag{A2}$$

and SST is the sum of squares about the mean

$$\mathrm{SST} = \sum_{i=1}^{n} w_i (y_i - \bar{y})^2 \tag{A3}$$

y_i, $\hat{y}_i$, $\bar{y}$, and w_i are the response value, predicted value, average response value, and weighting coefficient, respectively. The weighting coefficient w_i was set equal to 1 for all i. Additional details are provided in the Matlab Curve Fitting Toolbox User's Guide.[19]

Manuscript received May 2, 2013, revision received Oct. 26, 2013, and final revision received Jan. 8, 2014.